Construction of Lung Tumor Model for Drug Screening Based on 3D Bio-Printing Technology

Yadong Yang (yangyd76@163.com)
Hangzhou Medical College https://orcid.org/0000-0002-3108-8581
Geng Yang
Hangzhou Medical College
Xingzhu Liu
Hangzhou Medical College
Yimeng Xu
Hangzhou Medical College
Siyu Zhao
Hangzhou Medical College
Wenyuang Zhang
Hangzhou Medical College

Research

Keywords: 3D printing, 3D tumor model, A549 cells

Posted Date: August 6th, 2020

DOI: https://doi.org/10.21203/rs.3.rs-51190/v1

Version of Record: A version of this preprint was published at Journal of Biomaterials and Tissue Engineering on July 1st, 2021. See the published version at https://doi.org/10.1166/jbt.2021.2706.

Abstract

Background: The sensitivity of two-dimensional (2D) cultured cells to the drugs cannot effectively mimic the effect of the drug *in vivo*, although 2D cell culture is the most widely used model for drug screening. With the development of tissue engineering, people are committed to developing 3D tissue models that can better reflect the biology *in vivo*, and tend to be mass and miniaturized. In this study, three-dimensional (3D) bio-printing was used to develop an appropriate 3D model for screening sensitive anti-lung cancer drugs *in vitro*.

Methods: A549 lung cancer cells were mixed with sodium alginate/gelatin as bio-printing ink to fabricate a cell-laden hydrogel grid scaffold structure. The sensitivity of the printed 3D model to drugs was evaluated with eight anti-tumor traditional Chinese medicines (*Oldenlandia*、*Atractylodes*、*Mylabris*、*S. Barbata*、*Zedoary*、*Nigrum*、*Cremastra* and *Prunella*). The crude Chinese medicine was treated by water extraction and alcohol precipitation. A fluorescent live/dead staining was carried out at different time to assess the cell survival rate in the 3D scaffolds. MTT assay was used to determine the inhibitory rate of eight antitumor traditional Chinese medicines on A549 cell proliferation in 3D-printed lung tumor models and conventional 2D culture models. The data of each group were analyzed to clarify the difference between 2D and 3D cultures, and to evaluate the feasibility of 3D-printed lung tumor model as a drug screening model.

Results: The growth states of A549 cells on the 3D scaffolds were different from 2D culture. The effect of various traditional Chinese medicines on the proliferation inhibition of tumor cells was positively correlated with the drug concentration, The inhibition rate of 2D cell culture was higher than that of 3D cell culture. However, microscopic observation showed that there were more dead cells in 3D culture than in 2D culture. But the fluorescence value detected by EGFP labeled cells was consistent with the results of MTT.

Conclusions: We conclude that 3D printed lung tumor model can be used for drug screening. Before drug screening enters animal level, tissue level screening can be carried out by 3D printed tumor model.

1. Background

Antitumor drugs are mainly screened at four levels: the molecular, cellular, tissue, and animal levels. Currently, two-dimensional (2D) cell culture models are the most widely used models in preliminary screening. For example, cell proliferation activity is examined by the MTT method, and cell migration and invasion are assessed by the cell scratch experiment and Transwell assay. These experimental methods are simple and rapid with short experimental periods, and they have played a good role in advancing our preliminary understanding of the proliferation, migration, and invasion of tumor cells. Solid tumors, however, are 3D collections of cells, and detection methods using 2D plane model cannot generalize and simulate 3D space environment. Cells also quickly lose their intrinsic characteristics and functions [1], such as cell-to-cell and cell-to-matrix interactions, spatiotemporal signals, metabolic gradients, and mechanical

property constraints. Moreover, it is not possible to reflect malignant progression *in vivo*, such as hypoxia/necrosis, niche characteristics of tumor cells, and drug resistance of tumor cells in solid tumors [2,3]. Different cellular responses between 2D and 3D tumor models have been fully shown in terms of protein and gene expression, protein gradient spectra, cell signals, migration and invasion, morphology, proliferation, viability, and tissue and drug responses [4–6]. Studies have shown that the multicellular spheres formed by 3D cultures have inherent drug resistance or multicellular drug resistance, but their drug resistance disappeared in 2D cultures [7]. This might be why most anticancer drugs, even targeted drugs, have been shown to be effective *in vitro*, but have shown low therapeutic effect in clinical trials. According to the Biotechnology Innovation Organization (BIO), in 2016, for every 5,000 to 10,000 drug candidates that enter development, there were fewer than 10 that were released to the market by the Food and Drug Administration (FDA). Furthermore, perhaps only two of these drugs generated enough revenue to cover their research and development costs. Therefore, there is the "billion dollars over 10 years" argument for new drugs. Obviously, 2D cell models cannot meet the needs for in-depth research [8]. There are also species and genus differences in animal models, and the experimental results obtained cannot accurately predict the results in human patients [9]. Nude mouse models of transplanted tumors provide local tissue microenvironment, generating tumors that are closely similar tumor tissues *in vivo*. However, there are some disadvantages to these models, such as harsh feeding conditions, high price, and long experimental period. With the development of tissue engineering, researchers have committed to developing 3D tumor models that can better represent their biological characteristics *in vivo*. In drug experiments, 3D-printed tissue models have solved the problems with the above two models and may improve the efficiency of drug screening. It will bring huge social and economic benefits if the model was successfully developed.

3D bio-printed tissues and organs have attracted increasing attention. Nadav. Noor, et al [10] used a patient's retinal tissue to print a vascularized heart. The 3D-printed heart almost matched the patient's immunological, cellular, biochemical, and anatomical features. This method provides a wide application prospect for the customization of human tissues and organs as well as simulation of the human internal environment and anatomical structure for drug screening. In recent years, increasing number of studies have used 3D bio-printing technology to construct 3D *in vitro* models. For example, Zhao Yu et al. printed HeLa cells and hydrogels together to build a cervical tumor model [11]. Hee-Gyeong, Yi et al. printed a glioblastoma model by using a patient’s tumor cells, vascular endothelial cells, and the extracellular matrix of porcine brain tissue as print-ink. The response of the patient’s cells to radiotherapy and chemotherapy *in vitro* was observed using the model [12]. These studies confirmed that 3D bio-printing technology may provide a faster, simpler, and more economical models than animal models. In addition, these 3D models may present more precise simulation of the reaction of human organs to drugs, promoting continuous improvement of drug efficiency and providing convenience for drug screening *in vitro*. In individualized treatment of cancer, the establishment of a patient-specific cancer model using a patient's own tumor cells would allow effective drug screening and determination of the most suitable treatment plan for the patient, which would be an important direction of cancer treatment development in the future.

In this study, 3D bio-printing technology was applied to construct lung tumor models *in vitro* by mixing A549 non-small-cell lung cancer cells with gelatin/sodium alginate. The sensitivity of the 3D model to drugs was tested by using eight antitumor traditional Chinese medicines (TCMs). The findings of this study provided a new strategy for drug screening at the tissue level.

2. Methods

2.1 Preparation and treatment of traditional Chinese medicine

Eight types of TCM, which meet the standard of the 2015 edition of “the Pharmacopoeia of the People's Republic of China”, Bozhou, Anhui, China, were extracted by the same method. Briefly, 30 g of crude TCM was weighed and soaked in deionized water at 40°C for 1 h. The decoction was then boiled twice and concentrated to a final volume of 50 ml. The TCM components were divided into the alcohol-dissolved and alcohol-precipitated parts by the alcohol precipitation method (the alcohol content was more than 80%). The ethanol was then removed by heating the ethanol extract to 80℃ with a constant temperature magnetic stirrer. After evaporation, distilled water was added to make the final volume 6ml, that is, the crude drug concentration of all 8 kinds of traditional Chinese medicine was adjusted to 5g/ml. After filtering and sterilizing, the alcohol-soluble part was collected for subsequent experiments.

2.2 Cell preparation

A549 lung cancer cells were preserved in our laboratory. A stable A549-EGFP cell culture was established as follows. A549 cells at the logarithmic growth phase were prepared into a suspension of 5×10^4 cells/ml and seeded in six-well plates at 2 ml per well. Next, the supernatant was discarded after 24 h. After that, 10 μl lentivirus (Yeasen; Shanghai, China) at 1×10^8TU/ml titer was added to 1 ml of enhanced infection solution containing 5 μg/ml polybrene, and the mixture was added to cell well. The mixture was replaced with low-glucose Dulbecco’s modified Eagle medium (DMEM) (Gibco; Thermofisher, USA) containing 10% fetal bovine serum (Gemini; California, USA), 100 μg/ml penicillin and 100 μg/ml streptomycin (Gibco; Thermofisher, USA) after 24 h of infection. On the third day, transfection was observed under a fluorescence microscope (Ts2R-FL; Nikon, Japan). After the cells had overgrown with monolayer, they were digested and seeded into six-well plates (Corning, USA) at a concentration of 1×10^5 cells/ml. Puromycin was added at a final concentration of 1 μg/ml for screening after incubation at 37°C for 24 h, and the medium was replaced with fresh screening medium every 2 days for a total of 7 days. The surviving cells were amplified and cultured as A549-EGFP cells.

2.3 Preparation of printing materials

Prepare 10 ml of the mixed printing material containing 5% gelatin (Sigma, USA) and 8% sodium alginate (low viscosity; Sigma). The materials were packed into airtight containers and pasteurized. The 3D printing materials were placed at 4°C until use. The study of printed material characterization, see references 13[13].

2.4 Lung tumor model was constructed by 3D bio-printing (BioScaffolder, GeSiM, Germany)

A549-EGFP cells or A549 cells and printing materials were used as printing inks, respectively. The final concentration of the cells was 2×10^6 cells/ml. Under the control of computer-aided design and pneumatic drive, the printing inks were continuously printed out. The scaffold was crosslinked with 5% $CaCl_2$ solution and transformed from sol to gel in a few minutes. Through 3D bio-printing, cells and extracellular matrix materials were arranged in a specific space; thus, lung tumor models were directly assembled and placed into six-well culture plates. Next, an appropriate amount of complete L-DMEM was added to the models, which were then cultured at 37°C in a 5% CO_2 incubator (BB150; Thermo, USA).

Printing parameters: the printing needle had a diameter of 0.41 mm and extrusion pressure of 120 kPa. The side length of the scaffold was 5 mm, the layer height was 0.16 mm. Each scaffold had three layers with four bars per layer and 90° corner printing. The heating module is set to keep the printing cylinder at 37℃. The scaffold forming temperature was about 15℃.

The cytotoxicity of the printed scaffold (without cells) was studied in ref. 13[13].

There were approximately 1.50×10^4 cells on each scaffold. On the first day after cell printing, the number of cells on the scaffold in one field of view was calculated by using the image acquisition and analysis software of ImageXpress Microcope (Molecular Devices, USA). The z-axis layer sweep, with one sheet per 60 μm, defines a particle with a fluorescence intensity between 20,000 and 25,000 and size between 30-50 μm as a cell, and calculates the total amount of cells per field. Nine fields of view were observed per scaffold, and the total number of cells on the scaffold = the number of cells per field × 9. The cell viability after printing = the total number of cells on the scaffold/initial number of cells planted × 100%.

2.5 Observation of cell growth on three-dimensional scaffold

To determine whether all cells show the same growth pattern on the scaffold and to provide experimental data for the construction of personalized models, we selected three lines of tumor cells and scaffold materials to construct 3D models, observed the growth of various cells on the scaffold, and compared them with the 2D culture. Three lines of tumor cells, namely A549 (lung cancer cell), HepG2 (hepatoma cell), and SSMC-7721 (hepatoma cell) at the same concentration (2×10^6 cells/ml) were mixed with the same ratio of sodium alginate/gelatin, printed, and then cultured *in vitro* in complete L-DMEM for 3 weeks. After staining with calcein-AM (Solarbio; Beijing, China), cell growth on the scaffold was observed under a fluorescence microscope and the effects of cell migration and invasiveness on the growth of the scaffold were preliminarily investigated.

2.6 Drug screening test grouping

Eight TCMs were divided into eight groups, which were then divided into two groups：a 3D-printed lung tumor model group and a 2D-cultured A549 cell group, and five concentrations were set for each group, respectively 1.00, 0.50, 0.10,0.05 and 0 g/ml. Each concentration had three replicate wells. Because of the

complexity of TCM ingredients, we repeated the experiment at least three times. All cultures were performed in 96-well plates.

2.7 Screening and detection of A549 cell sensitivity in 2D and 3D cultures

Screening of A549 cell sensitivity to TCM in 2D culture

The MTT method was used to determine the growth and proliferation of A549 cells in a 2D culture. Briefly, A549 cells at 1×10^4 cells were inoculated in each well of 96-well plates and cultured for 1 day with different concentrations (1.00, 0.50, 0.10, and 0.05 g/ml) of *Oldenlandia*, *Atractylodes*, *Mylabris*, *S. barbata*, *Zedoary, Nigrum*, *Cremastra*, and *Prunella* solutions diluted in complete medium at 200 mL/well. Each concentration had three replicate wells. Changes in cell morphology were observed by microscopy after 48 h of drug treatment. At the same time, the supernatant was discarded, and 100 μL of 500 μg/ml MTT (Sigma, UAS) was added to each well, which was then incubated at 37°C in the dark for 4 h. The supernatant was discarded and 150 μL/well dimethyl sulfoxide was added to the well. The precipitated crystals were completely dissolved within 10 min by oscillating at room temperature, and the absorbance OD value of each well was detected at a wavelength of 490 nm by a microplate reader (Thermo, USA). From the absorbance, the cell proliferation inhibition rate of TCM at different concentrations and incubation time was calculated. The experiment was repeated four times, and the proliferation inhibition rate IR(%) = (OD value of the untreated group - OD value of the drug treatment group) / OD value of the untreated group × 100%.

Cell apoptosis and cell cycle were detected by flow cytometry (BD FACSCelesta, USA). A549 cells at 1×10^5cells/ml (without transfection with EGFP) were inoculated into six-well plates at 500 μl/well, and eight TCMs were added after 1 day of culture, with two concentrations for each TCM (1.00 and 0.10 g/ml) and three duplicate wells per concentration. The cells (including floating cells in the supernatant) were collected after 24 h of treatment. The cells were washed twice with Phosphate buffer saline (PBS), stained with annexin-V fluorescein isothiocyanate (FITC) and propidium iodide (PI) (Biovision, USA), and incubated in the dark for 5 min. The proportion of early apoptotic cells in PI-/FITC+ samples was detected on flow cytometry, and morphological changes after apoptosis were analyzed by the data of forward scatter (FSC) and side scatter (SSC). The data were analyzed by FlowJo (Version 10, BD).

The cells collected as described above were washed with precooled PBS, and then suspended in 1 ml PBS and vortexed. Next, 3 ml precooled anhydrous ethanol was slowly dropped on the suspension to a final concentration of 75%. The cells were fixed overnight at 4°C.The fixed cells were washed with precooled PBS, and an appropriate amount of RNase was added to its working concentration of 50μg/ml, then incubated at 37°C for 30 min. Subsequently, an appropriate amount of PI was added to a final concentration of 50μg/ml, and the cells were stained at 4°C for 30 min in the dark to determine the cell cycle.

Screening of sensitivity to TCM in three-dimensional culture of A549 cells:

The lung tumor model was printed to fit into a 96-well plate (5 mm side length, three layers, four strips in each layer, 0.16 mm in each layer). Each lung tumor model contained approximately 1.25×10^4 cells (owing to the large cell damage and high rate of cell death during the printing process, the initial concentration of the cells was slightly higher than that of the 2D culture). After 1 day of culture, different concentrations of *Oldenlandia*, *Atractylodes*, *Mylabris*, *S. barbata*, *Zedoary, Nigrum*, *Cremastra*, and *Prunella* were added to the cells. After 24 and 48 h of culture, changes in cell morphology after drug treatment were observed under a microscope. The state of A549-EGFP cells on the scaffold was observed under a fluorescence microscope and compared with that of cells grown in 2D culture. Surviving and dead cells on the scaffold were observed by Calcein-AM/PI staining of the A549 cells not transfected with EGFP. The inhibition rate of A549 cell proliferation in the 3D culture system was measured by the MTT assay or fluorescence intensity analysis.

2.8 Statistical methods

The SPSS13.0 statistical software package was used for statistical analysis. The experimental data were expressed as $\bar{x}\pm s$. Comparisons between groups were conducted, with $P<0.05$ indicating statistical significance.

3. Results

3.1 Eight anti-tumor traditional Chinese medicines :

as shown in Fig. 1

3.2 Establishment of stable A549-EGFP cell line

Three days after transfection of A549 cells, the cells had almost been transfected with EGFP. After screening with puromycin, EGFP expression in the cells was over 99%.

3.3 Lung tumor model was constructed by 3D bio-printing

The printed material characterization and the cytotoxicity of the printed scaffold was studied in ref.13[13]. After cross-linking, the printed 3D model changed in color from transparent to milky white (Fig. 2A and B), and the whole scaffold shrunk, with the side length reduced from 5 mm to 4 mm. The number of cells on the scaffold was approximately 1.16×10^4 cells at 1 day after printing, and the cell survival rate was approximately 77.33% (Fig. 2C and D). After culture for 20 days, the scaffold maintained a good morphological structure (Fig. 2E). After culture for 50 days, cracks appeared in the scaffold, as shown in Fig. 2F.

3.4 Observation of cell growth on the three-dimensional scaffold

All three kinds of cells were adherent to the wall in 2D culture (Fig. 3A2, B2, C2), while in the same scaffold materials, the growth state of the three cells was different. A549 cells were mainly scattered in

the scaffold (Fig. 3A1), HepG2 cells were tunneled in the scaffold, with cells densely accumulated in the tunnel (Fig. 3B1), and SSMC-7721 cells grew as "grape clusters" in the scaffold (Fig. 3C1).

3.5 Effect of eight alcohol extracts of TCM on 2D culture of A549 cells

Mylabris extract at all concentrations had an inhibitory effect on cell proliferation; treatment with this extract at high concentration led to almost no cells in the field of vision. A large number of dead cells floated in the supernatant. MTT results showed that at 0.05 g/ml, the other TCMs could not inhibit the proliferation of A549 cells, whereas the inhibitory rate of *Mylabris* extract on A549 cells was still 66.4%, $P < 0.005$. The alcohol extracts of *Oldenlandia*, *Atractylodes*, *Mylabris*, *S. barbata*, *Zedoary, Nigrum* and *Cremastra* inhibited the proliferation of A549 cells in a concentration-dependent manner; the higher the concentration of the drug, the more significant their inhibitory effect on cell proliferation. In a certain concentration range (0.10-1.00 g/ml), *Prunella* alcohol extract showed negative correlation with cell inhibition, and the cell morphology observation result was consistent with the MTT results. In this concentration range, lower drug concentration was associated with stronger cell-inhibitory effect; thus, the cells shrunk and were in poor status, and the number of cells decreased. After treatment with *Prunella* extract at 1.00 and 0.50g/ml, the cells were in good status, but the number of cells was less than that of the normal control. After treatment with *Prunella* extract at a concentration of 0.10 g/ml, the cells shrunk and the number of cells was significantly reduced. However, after treatment with *Prunella* extract a 0.05g/ml, the cells returned to their normal state. The specific inhibitory effects of the eight TCMs are shown in Fig. 4 and 5.

3.6 Apoptosis of A549 cells treated with eight ethanol extracts of TCM for 24 h

The histogram of FSC and SSC (FIG. 6A) showed morphological changes in the cells. Compared with that in the control group, the histogram of FSC shifted to the left and SSC shifted to the right in all other groups, except for the nigrum group. The results suggested that the cell size decreased and the number of intracellular particles increased after treatment with the drugs, which were consistent with the morphological changes in the apoptosis assay. The histogram of FSC left-shift in the *Atractylodes* and *Mylabris* groups was positively correlated with drug concentration. In addition to those in the *Mylabris* and nigrum groups, the histograms of SSC right-shift in the other six groups were positively correlated with drug concentration. The median fluorescence intensity of FSC and SSC in each group was statistically different from that of the control group ($P<0.05$), except for the median fluorescence intensity of FSC in the *Nigrum* 0.10 g/ml group, as shown in Fig. 6B.

Compared with that in the control group, the rate of early apoptosis in the treatment groups was significantly increased, except in the 1.00 g/ml *Oldenlandia* and *Zedoary* groups ($P<0.05$), as shown in Fig. 6C and D.

3.7 Changes in A549 cell cycle after treatment with eight TCMs for 24 h

Compared with that in the control group, the proportion of cells in the G0/G1 phase roughly decreased, that in the G2/M phase increased, and that in the S phase remained basically unchanged, which suggested that the cell cycle was changed after treatment with the drugs, and that it was blocked in the G2/M phase (Table 1).

Table 1.
Cell cycle distribution of A549 after treatment with different concentrations of eight TCMs for 24 h (n=3, $\bar{x}\pm s$).

Group		Cell cycle		
Traditional Chinese Medicine	concentration (g/ml)	G0-G1	G2-M	S
Oldenlandia	0.10	53.58±11.49	19.00±0.86*	26.05±9.77
	1.00	59.55±11.97	8.89±6.94	27.47±12.55
Atractylodes	0.10	61.99±4.71*	11.09±8.15Δ	22.75±11.48
	1.00	58.32±6.36*	20.99±4.49*Δ	22.32±10.26
Mylabris	0.10	40.73±11.02*	16.76±10.37	26.63±8.20
	1.00	52.85±15.64	19.66±4.59*	22.43±11.18
S. Barbata	0.10	45.40±15.11*	18.11±13.49	24.35±18.25
	1.00	54.38±15.06	24.92±6.42*	12.03±8.73*
Zedoary	0.10	55.64±4.36*	14.33±8.09	28.2±11.40
	1.00	54.78±6.78*	17.08±2.10*	28.04±5.13
Nigrum	0.10	64.25±6.15	15.06±12.14	27.45±0.01
	1.00	57.80±19.30	17.7±10.60	18.96±18.6
Cremastra	0.10	57.38±17.75Δ	17.08±8.99	16.01±13.79Δ
	1.00	29.54±5.24Δ*	15.49±6.09	50.09±4.01*Δ
Prunella	0.10	49.70±22.89	19.56±11.78	14.19±5.25
	1.00	49.00± 12.28*	18.16±12.80	32.06±16.23
Control	/	69.00±29.05	7.42±3.75	23.58±8.44

*P<0.05 compared with the control group;

Δ P<0.05 the comparison between different concentrations of the same drug.

3.8 Effect of eight alcohol extracts of TCM on 3D culture of A549 cells

After A549 cells cultured in 3D scaffold were treated with eight TCMs for 24 and 48 h, the proliferation inhibition rate of five TCMs (*Atractylodes*, *Mylabris*, *Zedoary*, *Cremastra*, and *Prunella*) was measured by fluorescence microscopy, and that of the other three TCMs (*Oldenlandia*, *S. Barbata*, and *Nigrum*) was detected by the MTT assay. The trend of cell proliferation inhibition rate obtained by the two methods was basically the same, reflecting the inhibitory effect of the TCMs on cell proliferation. However, the fluorescence value measured by the fluorescence method could cause larger error than that by MTT method.

The growth state of 3D-cultured cells on the scaffold was not as good as that of the 2D-cultured cells. A large number of cells died after treatment with the drugs (Fig. 7A); however, the MTT and fluorescence methods showed that the cell proliferation inhibition rate in the 3D culture was significantly lower than that in the 2D culture after treatment with high-concentrations of *Oldenlandia*, *Atractylodes,S. Barbata*, and *Zedoary* as well as after treatment with *Mylabris* and *Prunella* at each concentration ($P<0.05$). In 3D culture, *Nigrum* did not inhibit proliferation, but promoted proliferation. However, in 2D culture, its proliferation inhibitory rate was positively correlated with its concentration.

Each concentration of *Cremastra* exhibited inhibitory effect on the proliferation of A549 cells in 2D and 3D cultures, and showed a concentration-dependent effect, but there was no difference in the proliferation inhibition rate between A549 cells grown in 2D and 3D cultures ($P>0.05$). These results suggested that in 2D and 3D cultures, the inhibitory effect of the drug on cells was different, but the general trend was the same, except for *Nigrum* (Fig. 7B and C).

4. Discussion

In recent years, 3D tumor models have been widely used in *in vitro* research of tumors, and have become an indispensable and powerful tool for studies of drug resistance, drug toxicology, tumor treatment, and angiogenesis[14-16]. Especially in the field of antitumor drug screening, compared with solid tumor models implanted in animals, a 3D tumor model constructed *in vitro* has the advantages of good repeatability, short research period, and low research cost, and is less controversial in terms of animal ethics. Therefore, it has become increasingly popular to construct 3D tumor models *in vitro*. Over the past decade, researchers have been developing 3D cell culture systems, which are generally constructed using three technologies :(1) 3D hydrogel system. Hydrogels are composed of water, ECM protein and growth factors. It can be customized to meet specific needs and can be used for continuous culture of multiple cell lines. There are many related products and applications: Cultrex® 3D culture tools[17], VitroGel™3D hydrogel system[18], and HydroMatrix™ polypeptide hydrogel[19]. (2) Cell aggregation. No extra extracellular matrix proteins are required. The commercial products include: Perfecta3D® suspended drop culture plate, Corning extremely low adsorption plane, Microplates 3D petri dishes, etc; (3) 3D scaffold, which can provide a physical support, and cells can enter the scaffold to grow and perform functions. Scaffold materials are mainly divided into two categories: natural materials and synthetic materials. In this study, we adopted the third method. We use 3D bio-printing technology to mix A549 cells with gelatin/sodium alginate to construct a lung tumor model *in vitro*, and to test the sensitivity of this 3D model by using

eight antitumor TCMs. Our approach to construct 3D models not only has the advantages of 3D hydrogels system, but is also more economical than using commercial products to build 3D models. We can print large numbers of individual 3D models at a time for drug screening. 3D scaffolds made of synthetic materials such as polystyrene are hard, and cells can only grow on the surface of the scaffolds. Cells are mainly attached to the bottom of the well after inoculation, and only a few adhered to the scaffold.

The most common histopathological manifestation of lung cancer is adenocarcinoma. A549 cells are a commonly used cell model to study non-small cell lung cancer; thus, so we chose A549 cells as seed cells. The research of biomaterials has promoted the development of organ and tissue engineering using 3D bio-printing. At present, the most popular materials include natural and artificial materials. Sodium alginate is a natural polysaccharide that dissolves in water to form a viscous liquid. When calcium ions are added to sodium alginate, crosslinked deposition occurs. Under extremely mild conditions, stable thermal irreversible gel is formed rapidly, and this process hardly causes damage to cells in the gel [20, 21]. In this study, the cell survival rate on the scaffold at 1 day after printing was 77.33%, supporting this previous finding. This result also suggested that changes in temperature and pressure in the 3D-printing process caused low damage to cells. Gelatin is a natural water-soluble biodegradable polymer. Its structure is similar to the tissue structure of organisms; thus, it has good biocompatibility. Its degradation products are easy to be absorbed without inducing inflammatory reaction. It is a mixture of thermal reversibility; when the temperature changes, a phase transition behavior is presented. By taking advantage of the properties of gelatin, we mixed it with sodium alginate at a certain proportion. By changing the temperature in the printing process, gelatin solidified, improving the mechanical properties of the whole model and improving the weak molding ability of sodium alginate alone. The two materials had good biocompatibility and biodegradability. The experiment results revealed that the cells grew well on the scaffold. After *in vitro* culture for more than 50 days, the scaffold cracked and formed an insect-like degradation from the hole to the periphery, and the scaffold then began to degrade. Even at this time, large number of cells still survived on the scaffold. The results showed that the materials had good biocompatibility and were basically nontoxic to cells, which survived for a long time. The slow degradation of the scaffolds could provide long-term 3D growth environment for seed cells, and apply to drug screening with long experimental time.

Different cells had different growth modes on the 3D scaffold. It was found that not only cells of different tumor types (lung adenocarcinoma A549 cells as well as human liver cancer SSMC-7721 cells and HepG2 cells) had different growth modes on the scaffold but different liver cancer cell lines, SSMC-7721 and HepG2 cells, also had different growth modes. This might be related to the invasion and migration of cells. It was suggested that different 3D tumor models could be constructed by using the appropriate cells. The more aggressive the cells, the more they could grow inside the material; therefore, the growth of cells per unit area significantly increased in the 3D scaffold compared with that in the 2D culture. The cells were packed so tightly that the drugs could not reach the inner cells directly; only surface cells died after treatment with the drugs, and a large number of cells inside survived, which could explain why the

number of dead cells in 3D culture was significantly higher than that in 2D culture. However, the MTT assay showed that the proliferation inhibition rate of cells in 3D culture was lower than that in 2D culture. This indicated that the drug exerted more potent inhibitory effect on the proliferation of 2D-cultured cells. This result was consistent with the finding that the drugs that were effective in the 2D experiments showed significantly decreased effects in animal or clinical trials.

Cell proliferation inhibition experiments showed that cell proliferation inhibition rate of the TCMs was basically concentration-dependent; the higher the concentration, the stronger the cell proliferation inhibition rate. In 2D culture, however, we found one exception, namely *Prunella*. Cells grew well under the action of high concentration of *Prunella* extract, but large number of cells died and floated in the supernatant under the action of low concentration of *Prunella* extract. Microscopic observation and MTT results were very consistent. To investigate this phenomenon, an apoptosis assay was performed. We found that after 24 h of treatment with *Prunella* at 1.00 g/ml, the rate of early apoptosis was 42.5% (±11.7%) and the rate of death and late apoptosis was 6.62% (±7.45%), suggesting that early apoptosis was induced in large number of A549 cells. However, *Prunella* at 0.10 g/ml directly caused the death of A549 cells, with death and late apoptosis rate of up to 63.0% (±10.6%) (mainly dead cells, because floating cells were collected when the cells were harvested). Therefore, microscopic observation and MTT assay results showed the high cell mortality of low-concentration *Prunella*. Through cell cycle detection, we found that after treatment with the TCMs, the cells were blocked in the G2/M phase. Combined with the apoptosis experiment, it was found that the cells became smaller and the particles inside the cells increased owing to the drugs, which was consistent with the morphological changes in the apoptotic cells: in the early stage of nuclear pyknosis, chromosomes were set on the inner side of the nuclear membrane, nuclear fragmentation occurred, the density of cytoplasm and organelles increased, and the cell volume decreased. Almost all cells in each group showed consistent changes after treatment with the eight TCMs, and it was concluded that the cells underwent cell death mainly by apoptosis after treatment with the drugs.

At present, chemoradiotherapy has become the main treatment for tumors, but its therapeutic effect is limited and it causes great pain and serious adverse reactions to patients. In this context, medical experts place their hopes on the research of anticancer drugs from TCMs, Chinese medical therapies, and integrated therapies using Chinese and Western medicines. The research on anticancer drugs from TCMs has been widely carried out. The chemical composition of crude TCMs is complicated, and different extraction methods obtain different components of TCMs. Most crude Chinese medicines contain terpenes and polysaccharides, but the specific functions of these various components have not been clearly defined at present. Triterpenoids [22,23], flavonoids[24], and polysaccharides have clear antitumor effects[25]. Owing to their complex chemical composition, the mechanism of their antitumor effect is also diverse, thereby showing the "multi-component, multi-target"[26] characteristics. Lung cancer treatment through induction of lung cancer cell apoptosis with TCMs has also achieved satisfactory results. However, the study of TCM pathology and pathophysiological changes in lung cancer has not been

sufficiently thorough; therefore, it is urgent to discover a model that can provide precise simulation of the growth environment of cells *in vivo* to perform preliminary drug research.

5. Conclusion

To provide reference for the selection of sensitive TCMs and personalized treatment, in this study, eight TCMs (*Oldenlandia*, *Atractylodes*, *Mylabris*, *S. barbata*, *Zedoary*, *Nigrum*, *Cremastra,* and *Prunella*), to which lung cancers are relatively sensitive[27-34], were selected as model drugs. A549 lung cancer cells were assembled with 3D bio-printing technology to construct an *in vitro* 3D lung cancer model for sensitivity screening of TCM. The inhibitory rates of the eight TCMs were detected and compared with 2D culture. Cell proliferation experiment found that in the 2D culture and 3D model, the effect of drugs on cell destruction was different, and the effect of drugs on proliferation inhibition was relatively weaker in the 3D model than in the 2D culture, but the effect of the drugs was basically the same (except for *Nigrum*). This result suggested that the 3D-printed A549 cell model can be used to screen anticancer drugs at the tissue level, as it may provide detailed data for further drug screening experiments in animals.

Abbreviations

2D: two-dimension;

3D: three-dimension;

TCM: traditional Chinese medicine;

MTT: 3-(4,5-Dimethylthiazol-2-yl)-2,5-diphenyltetrazolium bromide

Declarations

Ethics approval and consent to participate

Not applicable.

Consent for publication

Not applicable.

Availability of data and material

All data generated or analysed during this study are included in this published article.

Competing interests

The authors declare that they have no competing interests.

Funding

This research was supported in part by grants from the Natural Science Foundation of Zhejiang Province of China (No. LY18H180010), grants from the Zhejiang Provincial Medical Science and Technology Plan Project of China (No. 2017KY307 and 2019KY364), and grants from Zhejiang Provincial Traditional Chinese Medicine Science and Technology Plan Project of China (No. 2016ZA044, and 2018ZA017)

Authors' contributions

Yadong Yang participated in designing researches, performing experiment, analyzing data, and writing the paper. Geng Yang, Xingzhu Liu, Yimeng Xu, Siyu Zhao and Wenyuan Zhang participated in the experiment implementation. All authors read and approved the final manuscript.

Acknowledgements

Not applicable.

References

1. Hirschhaeuser F, Menne H, Dittfeld C, West J, Mueller-Klieser W, Kunz-Schughart LA. Multicellular tumor spheroids: an underestimated tool is catching up again. J Biotechnol. 2010;148(1):3-15
2. Yang MY, Chiao MT, Lee HT, Chen CM, Yang YC, Shen CC, et al. An innovative three-dimensional gelatin foam culture system for improved study of Glioblastoma stem cell behavior. J Biomed Mater Res B Appl Biomater. 2015;103(3):618-28
3. Fischbach C, Chen R, Matsumoto T, Schmelzle T, Brugge JS, Polverini PJ, et al. Engineering tumors with 3D scaffolds. Nat Methods. 2007; 4(10):855-60
4. Levinger I, Ventura Y, Vago R. Life is three dimensional-as in vitro cancer cultures should be. Adv Cancer Res. 2014; 121:383-414
5. Wang C, Tang Z, Zhao Y, Yao R, Li L, Sun W. Three-dimensional in vitro cancer models: a short review. Biofabrication. 2014;6(2):022001
6. Ozbolat IT, Peng W, Ozbolat V. Application areas of 3D bioprinting. Drug Discovery Today. 2016;21(8):1257-71
7. Godoy P, Hewitt NJ, Albrecht U, Andersen ME, Ansari N, Bhattacharya S, et al. Recent advances in 2D and 3D in vitro systems using primary hepatocytes, alternative hepatocyte sources and non-parenchymal liver cells and their use in investigating mechanisms of hepatotoxicity, cell signaling and ADME. Arch Toxicol. 2013; 87(8): 1315-30
8. Hou X, Guo Q, Yang J, Shan W. Advances in 3D cell-based drug screening model research. Bulletin of Fermentation Science and Technology. 2018;47(1):52-7
9. Goodenberger ML, Jenkins RB. Genetics of adult glioma. Cancer Genet. 2012;205(12):613-21

10. Noor N, Shapira A, Edri R, Gal I, Wertheim L, Dvir T. 3D Printing of Personalized Thick and Perfusable Cardiac Patches and Hearts. Advanced Science. 2019;6(11):1900344.
11. Zhao Y, Yao R, Ouyang L, Ding H, Zhang T, Zhang K, et al. Three-dimensional printing of Hela cells for cervical tumor model in vitro. Biofabrication. 2014;6(3): 035001
12. Yi HG, Jeong YH, Kim Y, Choi YJ, Moon HE, Park SH, et al. A bioprinted human-glioblastoma-on-a-chip for the identification of patient-specific responses to chemoradiotherapy. Nature Biomedical Engineering. 2019;3(7):509-19
13. Yang YD, Yang G, Song YF, Xu YM, Zhao SY, Zhang WY. 3D Bioprinted Integrated Osteochondral Scaffold-Mediated Repair of Articular Cartilage Defects in the Rabbit Knee. J Med Bio Eng. 2020; 40(1): 71–81
14. Jang K, Sato K, Igawa K, Chung UI, Kitamori T. Development of an osteoblast—based 3D continuous-perfusion microfluidic system for drug screening. Analytical and Bioanalytical Chemistry. 2008;390(3): 825-832
15. Seano G, Chiaverina G, Gagliardi PA, di Blasio L, Sessa R, Bussolino F, et al. Modeling human tumor angiogenesis in a three-dimensional culture system. Blood. 2013;121(21):e129-137
16. Luca AC, Mersch S, Deenen R, Schmidt S, Messner I, Schäfer KL, et al. Impact of the 3D microenvironment on phenotype, gene expression, and EGFR inhibition of colorectal cancer cell lines. PloS One. 2013;8(3): e59689
17. Akoury E, Ahangar P, Nour A, Lapointe J, Guérard K P, Haglund L, et al. Low-dose zoledronate for the treatment of bone metastasis secondary to prostate cancer. Cancer Cell Int. 2019;19: 28.
18. Xiao M, Qiu J, Kuang R, Zhang BD, Wang W, Yu Q. Synergistic Effects of Stromal Cell-Derived factor-1α and Bone Morphogenetic protein-2 Treatment on Odontogenic Differentiation of Human Stem Cells From Apical Papilla Cultured in the VitroGel 3D System. Cell Tissue Res. 2019;378(2): 207-20
19. Ylärinne JH, Qu C, Lammi MJ. Scaffold-free approach produces neocartilage tissue of similar quality as the use of HyStem™ and Hydromatrix™ scaffolds. J Mater Sci Mater Med. 2017; 28(4):59.
20. Stanton MM, Samitier J, Sánchez S. Bioprinting of 3D hydrogels. Lab Chip. 2015; 15(15): 3111-5
21. Lee CS, Gleghorn JP, Won Choi N, Cabodi M, Stroock AD, Bonassar LJ. Integration of layered chondrocyte-seeded alginate hydrogel scaffolds. Biomaterials. 2007; 28(19): 2987-93
22. Bai YB, Li C, Zhou YM, Pi SL, Xia BH, Li YM, et al. Chemical constituents of triterpenoids from Prunella vulgaris and their antitumor activities. Chinese Traditional and Herbal Drugs. 2015; 46(24): 3623-9
23. Pei H, Qian SH. Studies on antitumor activity of two triterpenoids in Prunella vulgaris L. Strait Pharmaceutical Journal. 2011; 23(3): 43-5
24. Yang Y, Tantai J, Sun Y, Zhong C, Li Z. Effect of hyperoside on the apoptosis of A549 human non-small cell lung cancer cells and the underlying mechanism. Molecular Medicine Reports. 2017; 16(5): 6483-8.

25. Tian X, Wang P, Zhan N, Ren YY, Ming L, Li PY. Advances in Studies on Antitumor Effective Components of Chinese Herbal Medicines. Special Wild Economic Animal and Plant Research. 2010; 32(3): 73-6
26. Hao HP, Zheng CN, Wang G J. Thoughts and experimental exploration on pharmacokinetic study of herbal medicines with multiple-components and targets. Yao Xue Xue Bao. 2009; 44(3): 270-5
27. Zhao SY, Zhang JN, Wu DF, et al. Experimental study on treatment of compound *Hedyotic diffusa* in tumor-burdened mice. Practical Clinical Journal of Integrated Traditional Chinese and Western Medicine. 2014; 6: 20-22
28. Zhao HM, Zhu QJ, Zheng GJ, Zhang D, Zhang J. Extract of *Largehead Atractylodes Rhizome* on external inhibitor invasion of PG cells of human lung cancer. Jouranl of Shangdong University of Traditional Chinese Medicine. 2005; 29(6): 465-466, 486
29. Zhang WD, Zhao HR, Yan Y, Wang XH, Zhong ZH, Liu Y. Apoptosis induced by *Cantharidin* in human pulmonary carcinoma cells A549 and its molecular mechanisms. Chin J Oncol. 2005; 27(6):330-4
30. Wei PY, Pu HQ, Wei X, Li CG, Nong S. Apoptosis-inducing effect of *Scutellaria barbata* extract on human lung cancer SPC-A-1 cells and the expression of apoptosis associated genes. *Journal of Chinese Medicinal Materials.* 2007; 30(10):1270-3
31. Chen ZQ, Zhang YZ. Mechanism of inhibition of *Zedoary* polysaccharide on Lewis lung cancer in mice. Chinese Journal of Gerontology. 2015; 35(7):1925-7
32. Yu XB. Effects of extracts of *Nigrum* on immune function and vascular endothelial growth factor in lung cancer model mice. Journal of Chinese Physician. 2017; 19(7):1048-50
33. Gu YN, Wu YP. Clinical observation of 45 cases with Yin deficiency and heat poisoning syndrome of advanced lung cancer treated by *Cremastra* prescription. Journal of New Chinese Medicine. 2016; 48(5):205-7
34. Zhu JH, Jia XB, Zhang W. Research of lung cancer A549 cells apoptosis in *vitro* induced by ethanol extracts from *Spica prunellae.* Northwest Pharmaceutical journal. 2014; 29(6):598-602

Figures

Figure 1

Eight anti-tumor traditional Chinese medicines

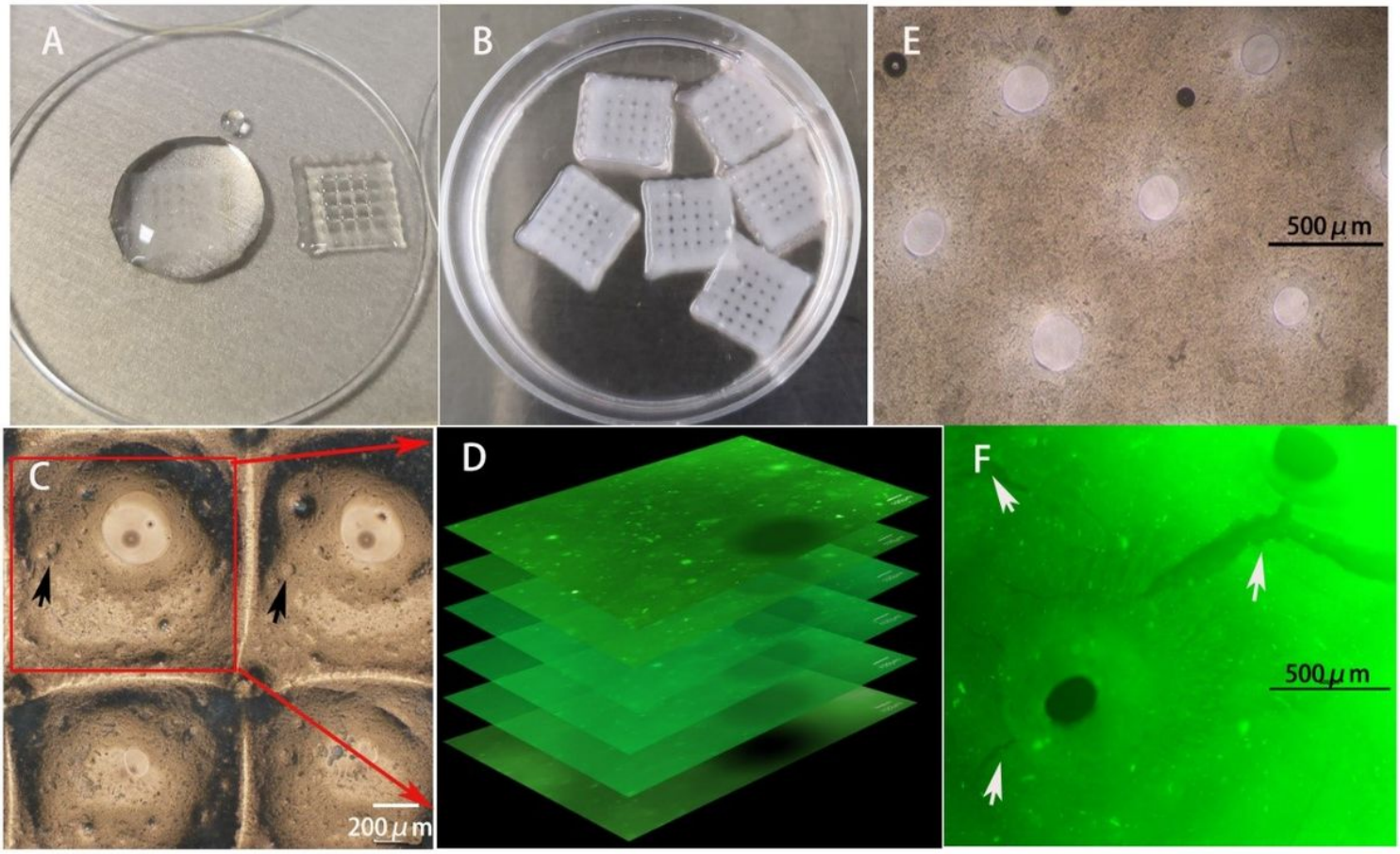

Figure 2

3D-printed scaffolds and their cells under microscope. A. 3D-printed scaffold is transparent before crosslinking. B. After cross-linking, the printed 3D model changed in color from transparent to milky white. C. The 3D scaffold was concave (×40), as observed under a phase-contrast microscope. Cell clusters on the surface of the scaffold are shown by the black arrow. D. Z-axis layer scanning overlay chart of a field of view as shown in the box in Figure C (×100). The numerous scattered highlights are cells on the scaffold. E. After culture for 20 days, the scaffold maintained a good morphological structure (×40). F. After the scaffolds and cells were cultured in vitro for 50 days, the scaffolds have shown significant degradation. The white arrow shows cracks in the scaffolds, and the green dots are scattered cells (Calcein-AM staining) (×40).

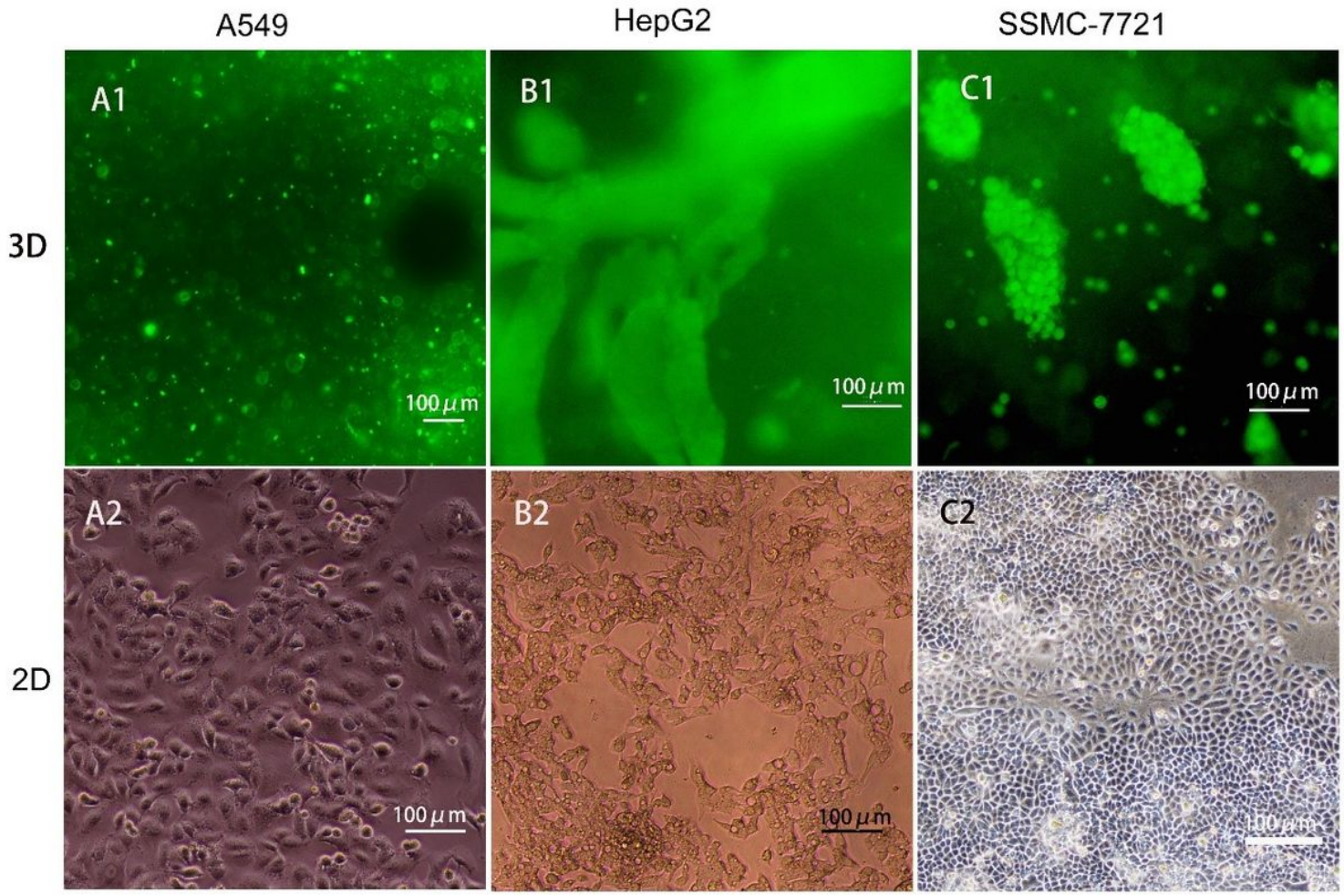

Figure 3

Comparison of cell morphology in a 3D culture and 2D culture (×100) Three types of tumor cells showed different growth patterns after 3 weeks of 3D culture in complete L-DMEM, while all cells showed adherent growth after 3 days of 2D culture. A1. A549 cells showed diffuse and scattered growth in 3D culture (Calcein-AM staining). A2. A549 cells were adherent to the wall and polygonal in shape in 2D culture. B1. HepG2 cells were tunneled in the scaffold, with cells densely accumulated in the tunnel (Calcein-AM staining). B2. HepG2 cells were adherent to the wall in 2D culture. C1. SSMC-7721 cells grew as "grape clusters" in the scaffold (Calcein-AM staining). C2. SSMC-7721 cells were adherent to the wall in 2D culture.

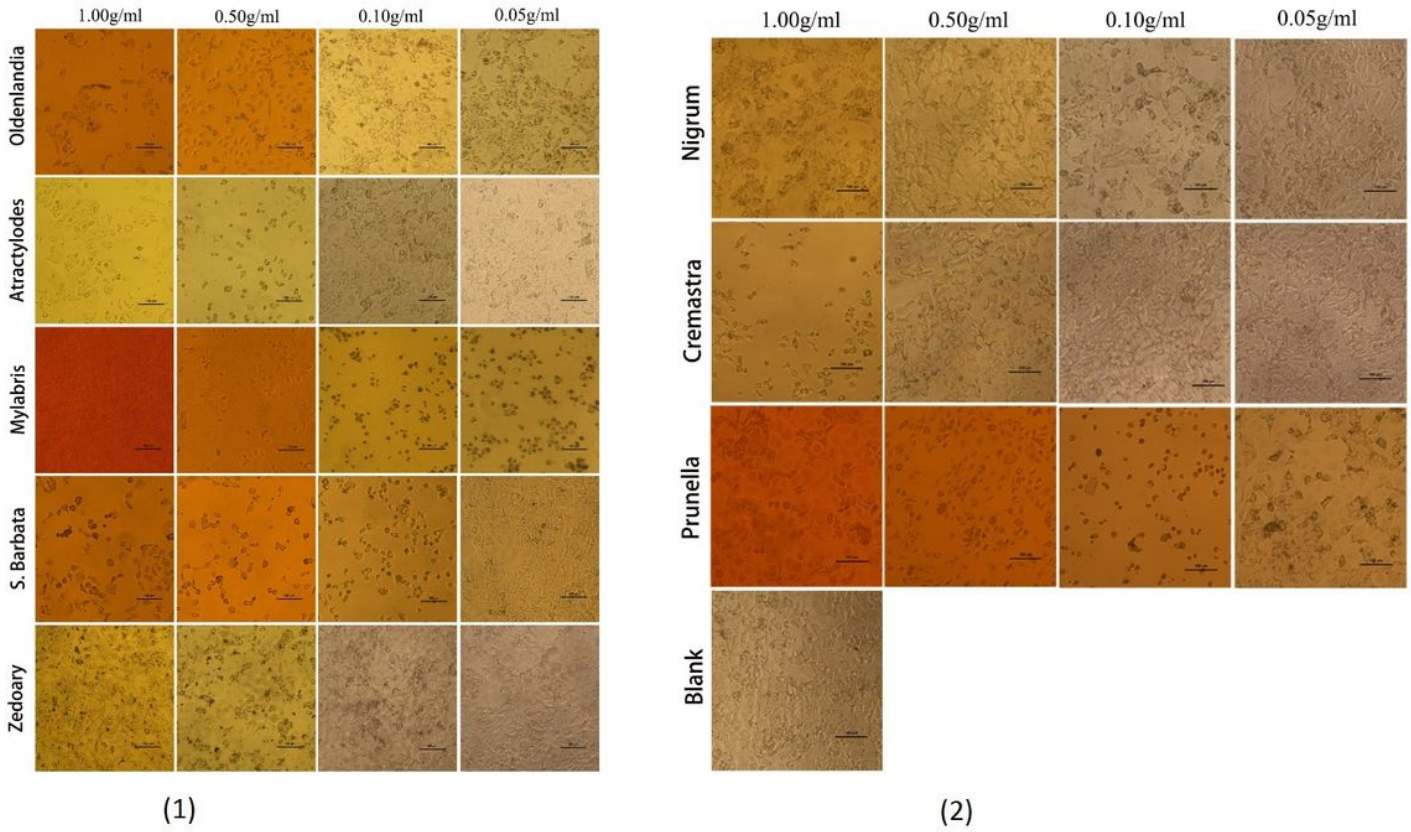

Figure 4

Changes in A549 cells morphology after treatment with eight ethanol extracts of TCM at different concentrations for 48 h (100×)

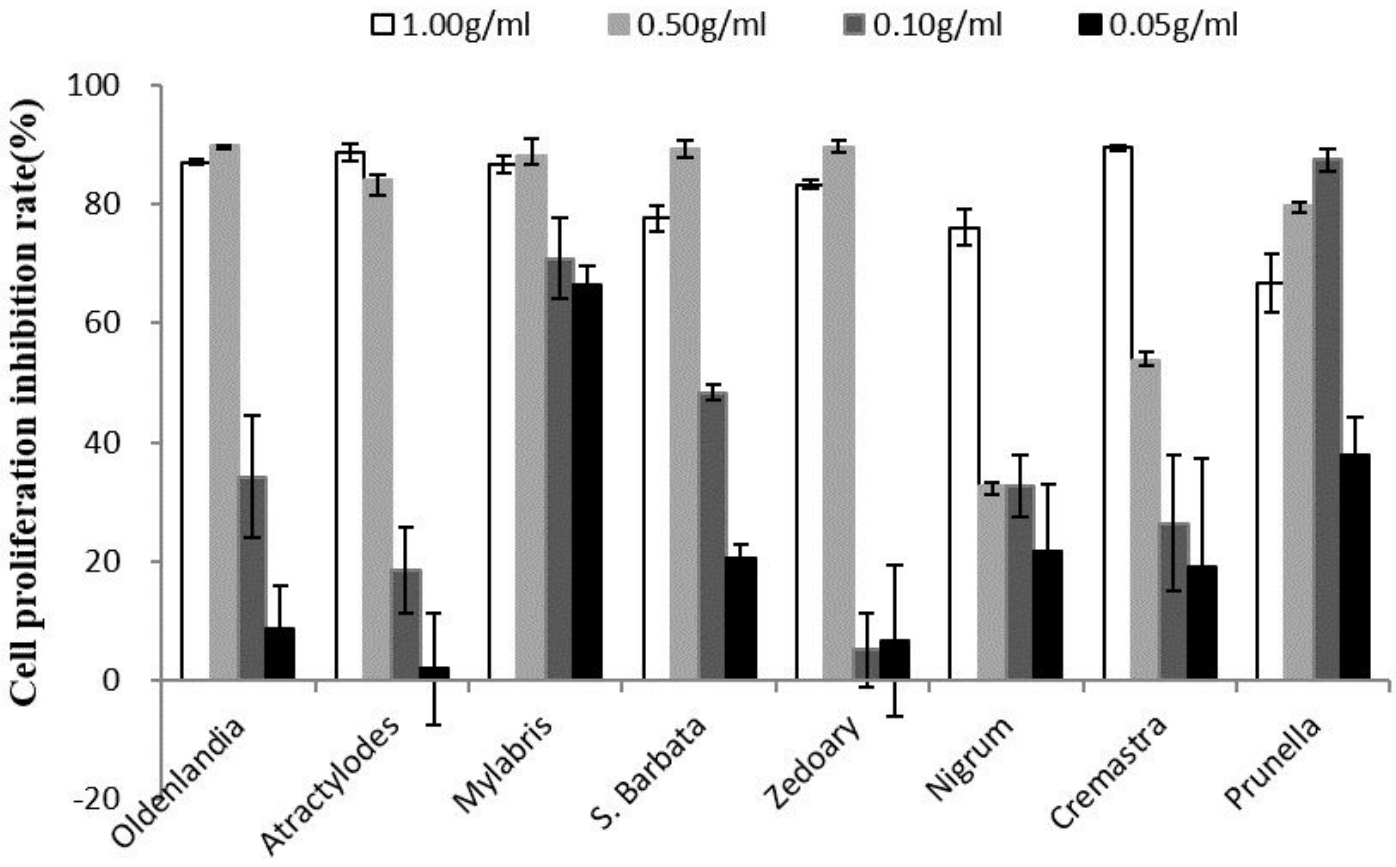

Figure 5

Inhibition rate of A549 cell proliferation in 2D culture was measured by MTT assay after treatment with eight ethanol extracts of TCM at different concentrations for 48 h

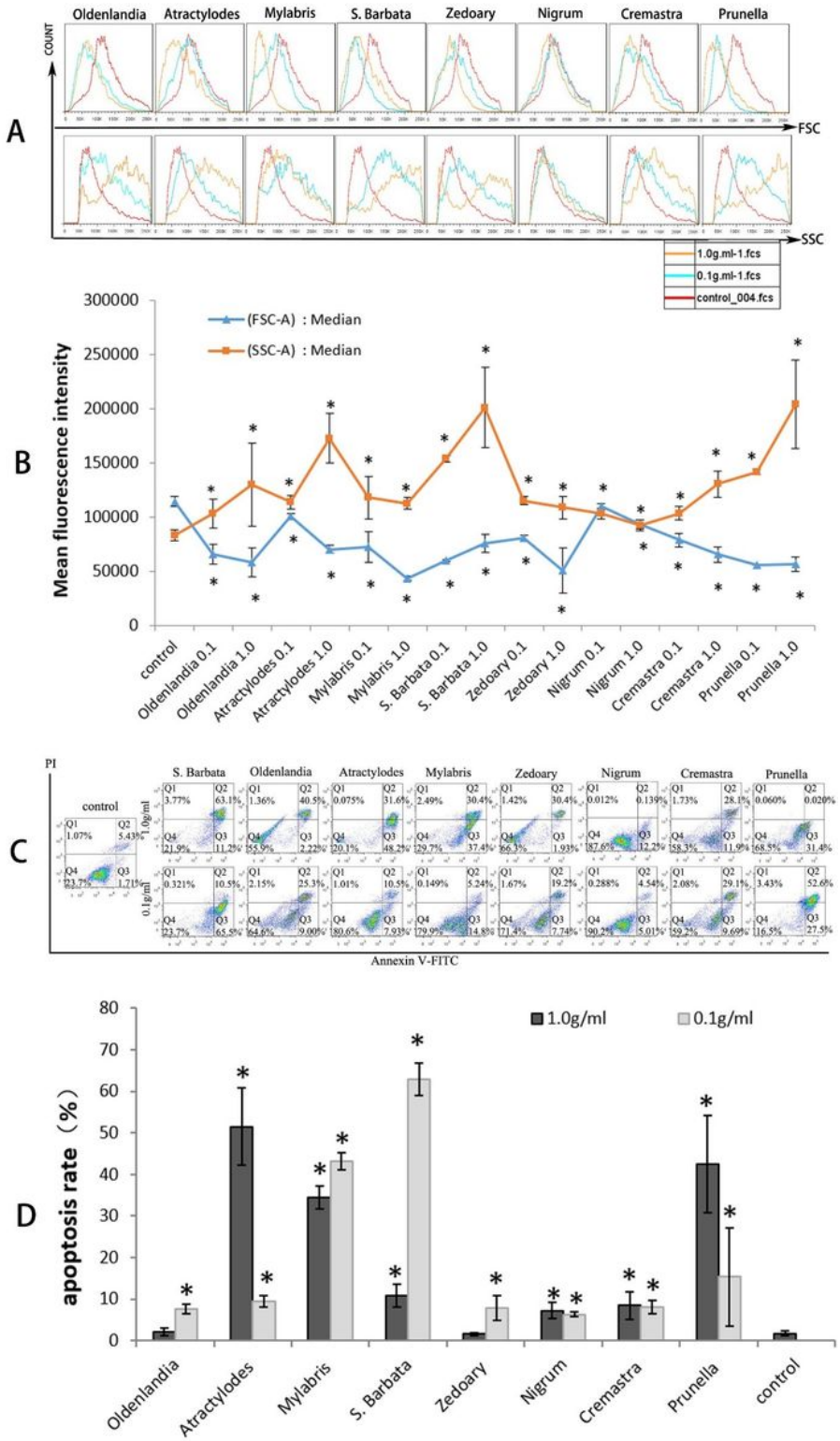

Figure 6

Apoptosis rate of A549 cells treated with eight TCMs at different concentrations for 24 h. *P<0.05 compared with the control group. A. Histograms of the average fluorescence intensity of FSC and SSC of the same drug concentration and the control group are overlaid. (The red line is the control group) B. Median fluorescence intensity of FSC and SSC in each treatment group was compared with that of the

control group. C. Flow cytometry scatter plot of apoptosis in each group. D. Early apoptosis rate of each group was compared.

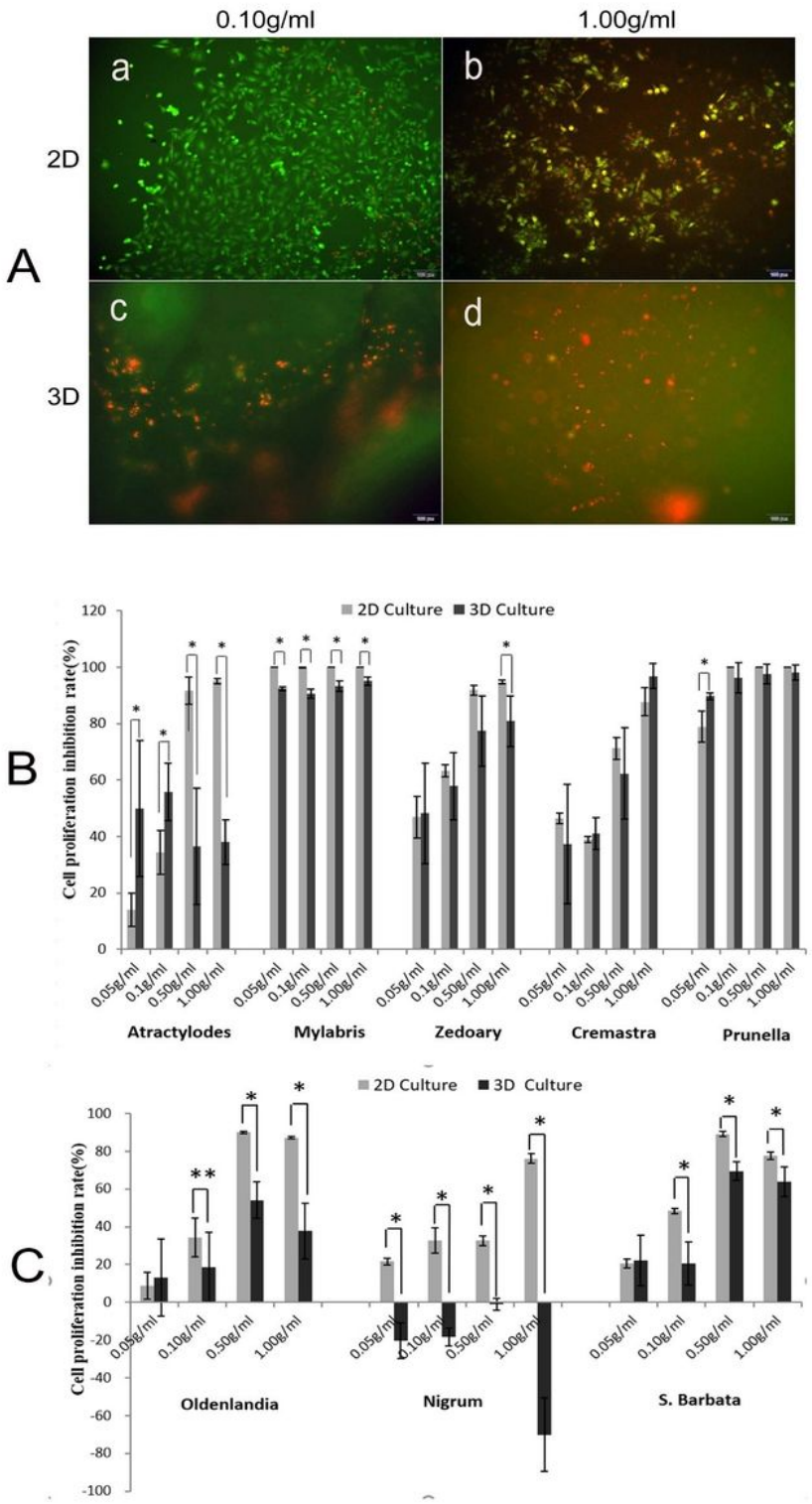

Figure 7

A549 cell growth in 2D and 3D culture was compared after treatment with different concentrations of eight TCMs for 48 h A. CAM/PI staining for determination of cell survival and death in 2D and 3D cultures after treatment with Atractylodes at concentrations of 0.10 g and 1.00 g/ml for 48 h (living cells, green

dots; dead cells, red dots) (40×) B. Proliferation inhibition rate of A549 cells grown in 2D and 3D culture for 48 h in the presence of different concentrations of five alcohol extracts of TCMs, as compared using the fluorescence method (*P<0.05) C. Proliferation inhibition rate of A549 cells grown in 2D and 3D culture for 48 h in the presence of different concentrations of three alcohol extracts of TCMs, as compared by using the MTT method (**P<0.05, * P<0.001)